Research Article

Multi-Objective Optimization of UV Spot Curing Technique of Slider-Suspension Attachment Process Using Response Surface Methodology Approach

Santi Pumkrachang*
Department of Industrial Engineering, Faculty of Engineering, King Mongkut's University of Technology North Bangkok, Bangkok, Thailand
Western Digital Company Limited, Ayutthaya, Thailand

Krisada Asawarungsaengkul
Operations Research and Engineering Management Research Center, Department of Industrial Engineering, Faculty of Engineering, King Mongkut's University of Technology North Bangkok, Bangkok, Thailand

Parames Chutima
Department of Industrial Engineering, Faculty of Engineering, Chulalongkorn University, Bangkok, Thailand

Abstract
The ultraviolet (UV) curing of slider-suspension attachment is going to change from a manual to an automated process. As a result, the bonding parameters of adhesive between slider and suspension needs to be optimized. This paper aims to study two output responses of the UV curable epoxy adhesive i.e., shear strength force and pitch static attitude (PSA) of the joint between slider and suspension in a head gimbal assembly (HGA). Four process parameters were investigated using response surface methodology (RSM) based on face-centered central composite design (FCCD). The RSM was applied to establish a mathematical model to correlate the significance of process parameters and the responses. Then, the based multi-objective was applied to determine a quadratic model and obtained the output maximization at 224 g of shear strength force and PSA value close to the target at 1.8 degrees. The input process parameters were optimized at 0.7 s of UV bottom cure time, 120 °C of UV dual side temperature, 5.0 s of UV dual side cure time, and 230 μm of adhesive dot size. The validation experiment showed a prediction response error of less than 7% of the actual value.

Keywords: Head gimbal assembly, UV curable epoxy adhesive shear strength force, Pitch static attitude, Face-centered central composite design

1   Introduction

Currently, epoxy adhesive is a widely used material for bonding different materials and assembly for industrial applications, automotive, microelectronic devices, medical products, aerospace industries. In hard disk drive (HDD), the epoxy-based adhesive is used to bond major component parts between slider and suspension. The bonding is a vital process of the head gimbal assembly (HGA) as display in Figure 1. In the bonding process, there are many quality characteristics requirements that are critical to the functionality of the HGA. In general, the destructive shear strength force testing of adhesive bonding is randomly performed. In addition, the non-destructive pitch static attitude (PSA) testing is measured with all samples. The appearance of the PSA, crown sensitivity and induced fly height are the critical process parameters that impact to the HGA quality and reliability in HDD. Normally, the HGA requires epoxy-based electrically
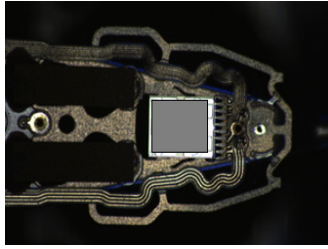
Figure 1: Head gimbal assembly (bonding area).

conductive adhesive due to the nanoscale physical contact area.

The epoxy adhesive bonding joint, the epoxy adhesive applications and the optimization of process parameters have been studied, discussed and reported during the past decade. The mechanical properties of the epoxy adhesive joint in the galvanized SAE1006 steel were discussed by Lin *et al.* [1]. The effect of temperature range and curing time on the joint strength of the epoxy adhesive were reported. The study of lap shear stress-strain curves and collapse modes of adhesive strength of joint cured under various temperatures was investigated by LeBono *et al.* [2]. The results indicated that the shear strength was significantly decreased from 2.72 MPa at 20 °C to 1.15 MPa at 0 °C. The microstructure and mechanical properties of ultraviolet (UV) curing and thermal stability of epoxy adhesive were discussed by Lee *et al.* and Aradhana *et al.* [3], [4]. In addition, the epoxy adhesive for timber-glass bonded at various temperatures were adopted to study load-displacement curves of shear under different environmental conditions [5]. A comparison of lap shear stress-strain adhesive joint obtained when the joint was on the radiofrequency (RF) electromagnetic field and infrared radiation (IR) were investigated by Gruener *et al.* [6]. It was demonstrated that the RF field was mainly contributed to a more rapid heat supply for the adhesive. Quan *et al.* [7] studied the mechanical performance of the adhesive joint of the reinforced poly-etherether-ketone (PEEK) and poly-phenylene-sulfide (PPS). The high-power UV irradiation, exposure time and intensity of the UV light were examined to achieve the better mechanical performance of the adhesive joint tensile lap-shear strength, load and displacement curves. Experiments on thermosetting adhesives with UV-assisted dispensing were presented by Schmidt and Zimmermann [8]. The results revealed that the

mechanical properties of Loctite 3217, Delo Monopox GE7985 and Delo Dualbond OB786 were higher than other chemical-based adhesives. The adhesive bonding of carbon-fiber/bismaleimide (BMI) joint using resistance heat transfer to cure thermally was examined by Rider *et al.* [9]. It was found that the thermal adhesive bonding can be performed accurately and can create a prediction model to compare the electrical resistance heat transfer on the composite laminate. Vallée and Adam [10] currently have been evaluated several techniques of induction heating of adhesive using Curie particles. The results revealed that the adhesive of 60 wt%, magnetite of 8 wt% and Mn-Zn-Ferrite of 3 wt% enhanced higher shear strength force of 12.11 MPa more than the adhesive of 60 wt%, magnetite of 4 wt% and Mn-Zn-Ferrite of 36 wt%.

The design of experiment (DOE) and the statistical analysis on the adhesive bond shear strength were investigated by certain researchers [1], [11]–[15]. The parameters that affected the adhesive bonding using factorial design were also studied by several researchers [1], [11]–[13], [15]. The regression model and the interaction of independent factors were significant. Additionally, the response surface methodology (RSM), was conducted as an optimization technique and quadratic terms model was used in describing the performance of the adhesive bonding shear strength and adhesive curing process. [14]. It was indicated that the desirability function of the RSM model could be used to find a mathematical model and an optimal solution for the mechanical and adhesive properties. Deeying *et al.* [16] studied the laser bonding technology of the HGA circuit connection bonding between slider pad and suspension pad using RSM. RSM was applied to manage the multi-objective in describing the optimal conditions that minimize the delta PSA and maximize the shear strength of the solder joint.

Due to the continuous improvement in HGA process, new product technology with areal densities near 1 TB/square-inch was developed. With this new product, the head fly height on the top of a media surface in HDD must equal 0.23 nm. The head fly height or fly height gap is the projected spacing between the reader element and the top of the media surface in HDD as shown in Figure 2. The PSA degree is another vital parameter for reading-writing data. The PSA is established as the suspension flexure torque relative to the suspension clamping surface (Datum A)
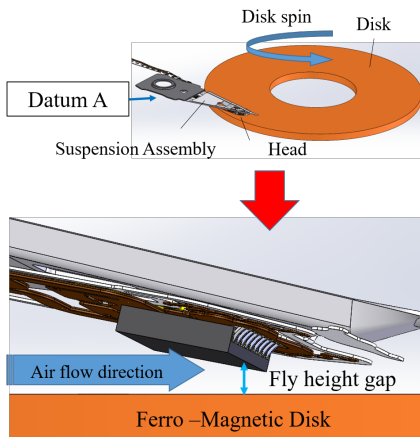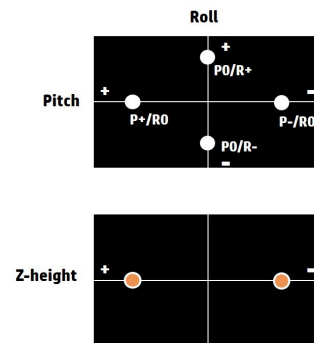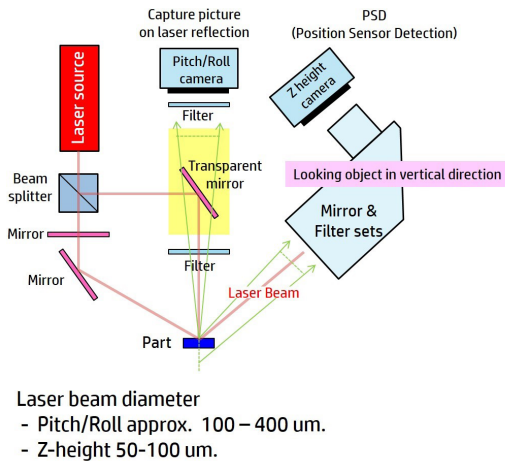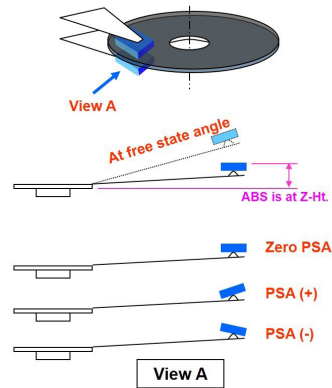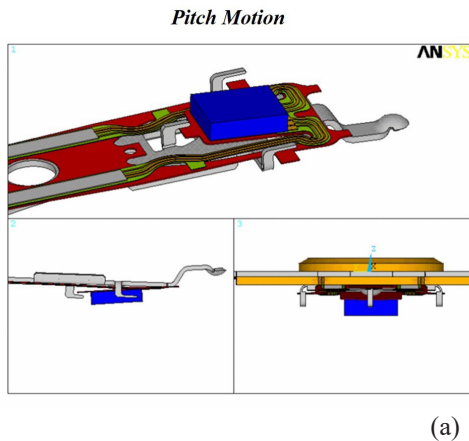
Figure 2: Fly height gap.

has been "elevated" to the slider height in Z direction (Z-Ht). Z-Ht is the simulated height between the suspension mounting surface to the top of ferromagnetic disk, which can be depicted in Figure 3.

The challenge of further improve this technology is the heat bonding parameters of adhesive between slider and suspension. The study is limited to the existing products and its component. Its application is critically important. The UV spot curing technique applied for the purpose of curing the epoxy adhesive-bonded to replace the conveyorized infrared oven technology is shown in Figures 4 and 5. UV spot curing units are composed of bottom side UV ray emitter to tag cure and hold the slider alignment while the dual side curing would fully cure the adhesive underneath the shade of

(a)

(b)

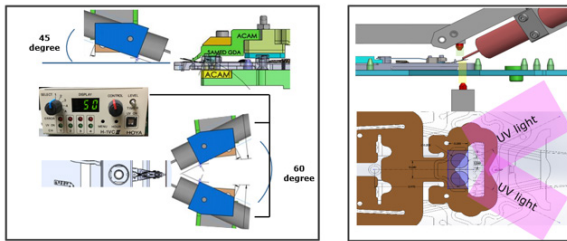**Figure 3**: (a) Pitch static attitude (PSA) (b) methodological technique to measure PSA.

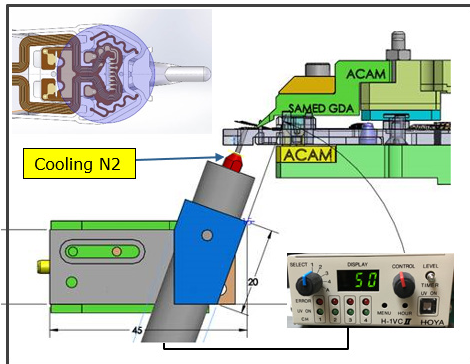**Figure 4**: Dual side UV emitter design for quick spot curing of adhesive.

Figure 5: UV design for bottom curing of adhesive.

Figure 6: Equipment used to measure the copper coil temperature inside a slider.

slider and stainless steel suspension. The UV guides were installed inside the assembly machine surrounding the HGA component. The proper orientation of the UV ray emitter is essential to the resultant energy to epoxy adhesive. The purposes of this replacement are to improve the capacity, reduce work in process material (WIP) and space for a production line. The two bonding parameters that shall be achieved are the PSA degree to be as close to the target value of 1.78 degrees and the shear strength force of the adhesive bonding as high as possible.

This paper aims to achieve the mentioned targets of the two process responses using RSM and multi-objective optimization. The four bonding parameters are the UV bottom curing time, UV dual side temperature, UV dual side curing time, and dot size UV curable epoxy adhesive.

2 Research Methodology

2.1 *Experimental procedure*

The HOYA H-1VCII UV at the intensity of 15–20 W/cm^2 was used to obtain the curing temperature of 90–150 °C to investigate the performance of the two bonding parameters. The curing temperature was set at the maximum of 150 °C because at the temperature over 160 °C, the magnetic device in slider for reading-writing data is damaged. The actual temperature was measured by a specially designed equipment to measurement the in-coil copper connector inside a slider as shown in Figure 6. The UV spot bottom side temperature was kept at 120 °C throughout the experiment.

The UV curable epoxy adhesive U-1499F supplied by Chemitec Technology, Japan was used. A shear test gauge used for this experiment was manufactured by Mecmesin Limitted, UK. Its specified resolution was 0.001 N as depicted in Figure 7(a). The PSA measurement equipment system supplied by Genetec Technology, Malaysia is shown in Figure 7(b).

The experimental process was intended to identify key process parameters for slider-suspension attachment of HGA for the new automated UV spot curing of the UV curable epoxy adhesive. The fractional factorial design screening was done prior to this optimization to get low(–1) and high(+1) level value. Four process parameters were focused. Each factor is defined as follows:

1) UV bottom curing time (A): UV bottom curing time is the time used to cure the surface of the adhesive to make sure the bonding position is in the correct position according to the fly height design XY location.

2) UV dual side temperature (B): Temperature indicates the heating source used to cure the UV curable
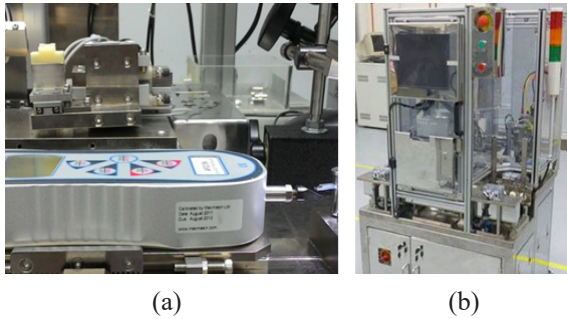
(a)

Figure 7: Images show (a) shear test equipment and (b) PSA measurement equipment to measure the shear strength force and PSA of adhesive bonding joint, respectively.

epoxy adhesive. It is a common factor that affects the curing of the UV curable epoxy adhesive, which applies to examine the peel strength at various curing conditions and derive the correlation between the adhesive force and the curing percentage.

    3) UV dual side curing time (C): UV dual side curing time is the time of the performing energy, which provides significance to the increase of the heat input.
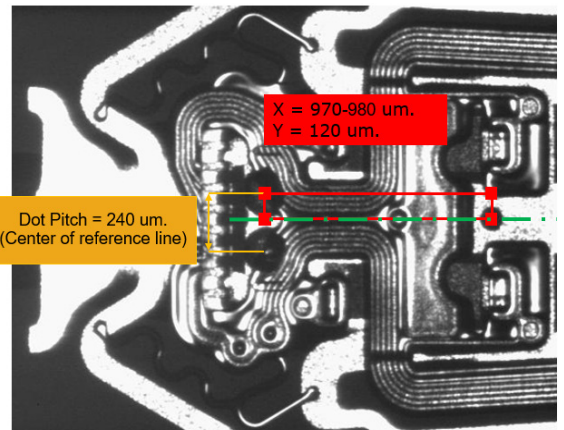
    4) Dot size (D): Dot size is the diameter of UV curable epoxy adhesive measured by machine vision as shown in Figure 8(a). However, the appearance of the adhesive bonding pattern after slider-suspension attachment is also inspected as shown in Figure 8(b). The defect based on the pattern after the slider-suspension attachment is unacceptable because it has a significant effect on the fly height performance of the HGA.

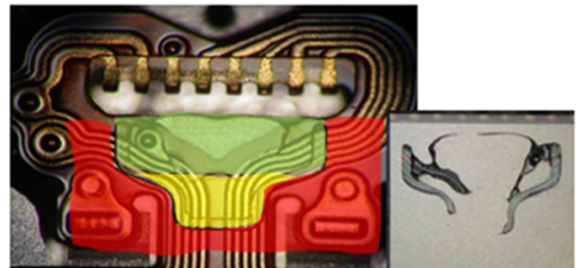## 2.2 *Response surface methodology (RSM) and experimental planning*

The face-centered central composite design (FCCD) was applied as the experimental design for RSM analysis. RSM is considered to be more suitable to explain the comparison between the key factors and the responses. In statistics, the response surface model can be expressed as in Equation (1):

$$y = \beta_0 + \sum_{i=1}^{k} \beta_i x_i$$

$$+ \sum_{i=1}^{k} \beta_{ii} x_i^2 + \sum_{i}^{k} \sum_{j}^{k} \beta_{ij} x_i x_j + \varepsilon; \quad i \neq j, i < j \quad (1)$$

where x_i and x_j are independent variables and y is the

(a)

(b)

Figure 8: Dot size diameter location and adhesive bonding pattern after slider-suspension attachment.

response variables, $\beta_0, \beta_i, \beta_{ii}, \beta_{ij}$ are constant term, linear coefficient, second-order-polynomial coefficient and interaction coefficient, respectively.

Table 1: Table placement in one column

Factor	Unit	Symbol	Levels		
			−1	0	1
UV bottom curing time	s	A	0.6	0.7	0.8
UV dual side temperature	°C	B	90	120	150
UV dual side curing time	s	C	3	4	5
Dot size	μm	D	190	210	230

    The FCCD of the four factors is summarized in Table 1. The FCCD of the variables for the shear strength force and PSA of UV curable epoxy adhesive of the joint recorded responses are tabulated in Table 2.

Table 2: Experimental design matrix and recorded responses

Run Order	UV Bottom Curing Time (A)	UV Dual Side Temperature (B)	UV Dual Side Curing Time (C)	Dot Size (D)	Shear Strength Force	PSA
1	0.6	90	3	190	140.73	1.96
2	0.6	120	4	210	192.22	2.42
3	0.8	90	3	190	143.19	1.80
4	0.7	90	4	210	160.33	2.40
5	0.7	120	4	210	199.69	2.50
6	0.7	120	4	210	201.45	2.56
7	0.7	120	4	210	196.76	2.36
8	0.6	90	5	190	159.46	2.30
9	0.6	150	5	230	212.80	2.10
10	0.8	90	3	230	182.39	2.27
11	0.6	90	5	230	208.66	2.22
12	0.7	120	5	210	205.69	1.78
13	0.8	150	5	190	166.88	2.15
14	0.7	120	4	210	192.62	2.33
15	0.7	120	4	210	185.35	2.39
16	0.8	150	5	230	210.65	1.90
17	0.7	120	4	210	189.50	2.43
18	0.6	150	3	230	195.11	1.99
19	0.6	90	3	230	177.57	2.14
20	0.8	90	5	190	153.67	1.98
21	0.8	90	5	230	185.63	1.79
22	0.7	120	4	210	190.67	2.40
23	0.8	150	3	230	200.33	2.38
24	0.6	150	5	190	147.66	2.42
25	0.7	150	4	210	200.45	2.40
26	0.6	150	3	190	150.40	1.65
27	0.7	120	3	210	175.64	1.80
28	0.8	120	4	210	216.88	2.54
29	0.7	120	4	230	211.53	2.34
30	0.8	150	3	190	151.40	2.05
31	0.7	120	4	190	167.36	2.37

2.3 *Multi-response desirability function of process parameters*

The desirability function approach is applied to optimize multiple responses. Minitab 17 can compute the optimization and mathematical transformation based on the desirability function [17]. The relationship between UV curable epoxy adhesive shear strength force of the joint and PSA on the HGA based on the combination of the multiple responses and optimization of the process parameters. The function transformation was ranged from 0 to 1, $d_i \in [0,1]$. The $d_i = 0$ denoted the least weight to the target and 1 give a higher weight response toward the target [18].

The functional objective of the overall desirability function is defined as Equation (2) for maximization and Equation (3) for minimization.

$$d_i = \begin{cases} 0; & y_i < L \\ \left[\dfrac{(y_i - L)}{(T - L)}\right]^{w_i}; & L \le y_i \le T \\ 1; & y_i > T \end{cases} \quad (2)$$

$$d_i = \begin{cases} 0; & y_i < U \\ \left[\dfrac{(U - y_i)}{(U - T)}\right]^{w_i}; & T \le y_i \le U \\ 1; & T \le y_i \end{cases} \quad (3)$$

The weight (w_i) can be assigned to weigh the desirability function ranged between 0 to 1. The simultaneous objective function for the significance of the overall desirability function (D) can be defined as Equation (4).

$$D = \left(d_1 \times d_2 \times ... d_n \right)^{\frac{1}{n}} = \left(\prod_{i=1}^{n} d_i \right)^{\frac{1}{n}} \quad (4)$$

Where n is number of response variables and d_i is the desirability function for the response variables.

3 Results and Discussion

In order to validate the relationship of the process input parameters and response variables that effects the UV curable epoxy adhesive shear strength force and PSA of joint on the HGA, the analysis of variance (ANOVA) is important decision support tool to determine the significance of the process input parameters. The multi-objective optimization was performed using the desirability function approach. Minitab 17 was fitted with the optimization based on the desirability function. All 31 runs of treatment combinations were carried out in a random order in the matrix as summarized in Table 3. All observations were tested and recorded for statistical analysis. ANOVA was conducted to show the significance of the model terms. The probability values (p-value) should be less than 0.05 to consider the model terms to be significant.

Table 3: Analysis of variance for the quadratic model of the UV curable adhesive shear strength force of joint.

Source	DF	Adj SS	Adj MS	F-Value	*p*-value
Model	4	13764.7	3441.18	43.17	0.000
Linear	3	10921.5	3640.50	45.67	0.000
B	1	854.9	854.91	10.73	0.003
C	1	1002.6	1002.62	12.58	0.002
D	1	9064.0	9063.96	113.72	0.000
Square	1	2843.2	2843.23	35.67	0.000
B*B	1	2843.2	2843.23	35.67	0.000
Error	26	2072.4	79.71		
Lack-of-Fit	20	1869.4	93.47	2.76	0.106
Pure Error	6	203.0	33.84		
Total	30	15837.1			

$R^2 = 0.869$; adjusted $R^2 = 0.849$; predicted $R^2 = 0.819$

However, model terms are insignificant, which the lack of fit occurred from noise (p-value is larger than 0.05) can be implied. The significance of the models of each response and the coefficients that applied to create the regression and quadratic mathematical models can be written as reduced model terms.

3.1 Analysis of the shear strength force of joint of the UV curable epoxy adhesive

As can be seen in Table 3, the p-value from the ANOVA analysis of the UV curable epoxy adhesive shear strength force of joint indicates the probability of less than 0.05. This can be interpreted that the dot size, UV dual side temperature, UV dual side curing time, and the quadratic effect on the UV dual side temperature with the determination coefficient are

$R^2 = 0.869$, adjusted $R^2 = 0.849$ and predicted $R^2 = 0.819$. The R^2 values are closed to 1, which can be considered that the response of the regression is the quadratic polynomial term. In addition, the power of the prediction is in reasonable agreement and adequate precision model discrimination within the confidence limit.

The quadratic polynomial model developed for the uncoded factors can be written as Equation (5) as follows:

$$Y_s = -409.3 + 5.405B + 7.46C + 1.122D - 0.2156B^2 \quad (5)$$

The variable Y_s is the UV Epoxy adhesive shear strength force of the joint.

3.2 Characterisation of the PSA effect

The ANOVA results for the mechanical properties of PSA is summarized in Table 4. The model terms are considered significant because the p-value of the interaction terms and quadratic terms contain the hierarchical model are less than 0.05. However, the main effects themselves are insignificant but those terms have to be kept in the model. The statistical technique reduces the term to establish to a hierarchical model is recommended and therefore applied in this analysis.

The adequacy value of the ANOVA is indicated by the determination coefficient of $R^2 = 0.916$, adjusted $R^2 = 0.881$, and predicted $R^2 = 0.795$, which are well fitted and close to 1. The lack of fit is insignificant relative to the model. The final quadratic model to obtain the uncoded unit for the prediction of PSA is as Equation (6) as follows:

$$Y_{PSA} = -4.57 - 22.95A - 0.01571B + 6.411C$$
$$+ 0.02825D + 17.83A^2 - 0.5117C^2$$
$$+ 0.02292AB - 1.238AC - 0.00675CD \qquad (6)$$

Where, Y_{PSA} is the predicted PSA value.

Table 4: Analysis of variance for the PSA quadratic model

Source	DF	Adj SS	Adj MS	F-Value	*p*-value
Model	9	1.85592	0.206214	25.58	0.000
Linear	4	0.03947	0.009868	1.22	0.331
A	1	0.00642	0.006422	0.80	0.382
B	1	0.00180	0.001800	0.22	0.641
C	1	0.02000	0.020000	2.48	0.130
D	1	0.01125	0.011250	1.40	0.251
Square	2	1.20420	0.602100	74.70	0.000
A*A	1	0.11029	0.110287	13.68	0.001
C*C	1	0.90868	0.908682	112.73	0.000
2-Way Interaction	3	0.61225	0.204083	25.32	0.000
A*B	1	0.07563	0.075625	9.38	0.006
A*C	1	0.24503	0.245025	30.40	0.000
C*D	1	0.29160	0.291600	36.18	0.000
Error	21	0.16927	0.008061		
Lack-of-Fit	15	0.13030	0.008687	1.34	0.379
Pure Error	6	0.03897			
Total	30	2.02519			

$R^2 = 0.916$; adjusted $R^2 = 0.881$; predicted $R^2 = 0.79$

3.3 *Response surface analysis of UV curable epoxy adhesive shear strength force of joint*

The combined effects of UV dual side temperature and UV dual side curing time on the UV curable epoxy adhesive shear strength force of the joint is shown in Figure 9. The joint shear strength force tends to increase to the maximum at 123 °C and the curing time of 5 s. The dot size of the UV curable epoxy adhesive was kept constant at 210 μm.

When the UV dual side temperature was held at 120 °C, it is evident from Figure 10 that the UV curable epoxy adhesive shear strength force of the joint increased directly with the dot size diameter and the UV dual side curing time. It can be observed from the plot that the increasing dot size diameter and UV dual size curing time effects the area of the UV curable epoxy adhesive to hold the bonding between slider and suspension.
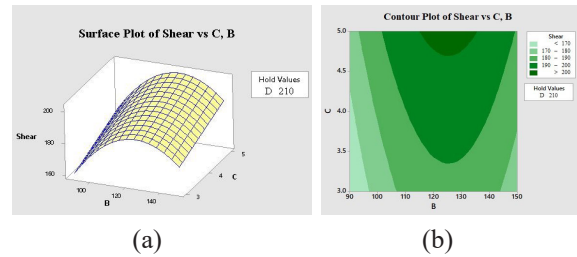

(a)   (b)

Figure 9: Relationship between the UV dual side temperature and UV dual side curing time on the UV curable epoxy adhesive shear strength force of joint (a) response surface plot and (b) contour plot.
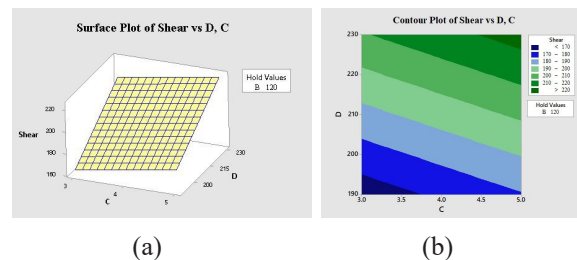

(a)   (b)

Figure 10: Relationship between the UV curable epoxy adhesive dot size diameter and UV dual side curing time on the UV curable epoxy adhesive shear strength force of joint (a) response surface plot and (b) contour plot.
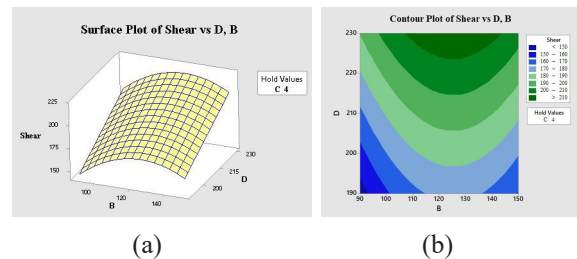

(a)   (b)

Figure 11: Relationship between the UV curable epoxy adhesive dot size diameter and the UV dual side temperature on the UV curable epoxy adhesive shear strength force of joint (a) response surface plot and (b) contour plot.

Figure 11 shows the relationship between the UV curable epoxy adhesive dot size diameter and the UV dual side temperature on the UV curable epoxy adhesive shear strength force of the joint. The UV curable epoxy adhesive shear strength force increases with the increasing dot size diameter and the UV dual side temperature. It is clear that the UV curable epoxy
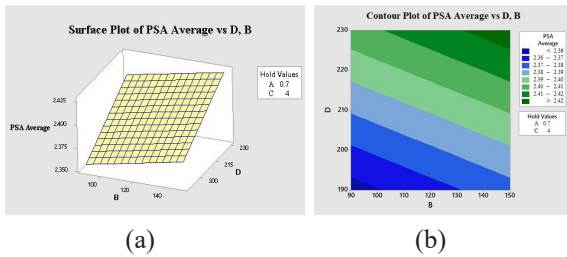
(a)   (b)

Figure 12: Relationship between the UV curable epoxy adhesive dot size and UV dual side curing time on the PSA (a) response surface plot and (b) contour plot.
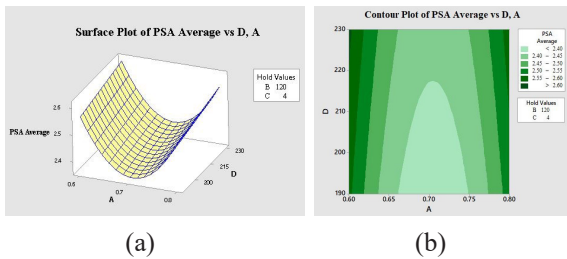

(a)   (b)

Figure 14: Relationship between the UV curable epoxy adhesive dot size and UV dual side curing time on the PSA (a) response surface plot and (b) contour plot.

(a)   (b)

Figure 13: Relationship between the UV curable epoxy adhesive dot size and UV bottom curing time on the PSA (a) response surface plot and (b) contour plot.

(a)   (b)

Figure 15: Relationship between the UV dual side curing temperature and UV bottom curing time on the PSA (a) response surface plot and (b) contour plot.

adhesive area was increased and the temperature for the UV dual side causes a completely cure UV curable epoxy adhesive to hold the bonding between slider and suspension.

3.4 *Response surface analysis of PSA in HGA process*

PSA is a critical characteristic for the fly height as low as 0.23 nm, which impacts the HGA quality and reliability. A 3-dimensional surface plot was employed to find the characteristics of the interaction effect between two performance input parameters.

Figure 12. is a response surface plot of the UV bottom curing time at 0.7 s and UV dual side curing time at 4 s, which were kept as a constant. It was founded the PSA is proportionally increased to the increasing of the diameter of dot size and the UV dual side curing temperature.

In Figure 13, the UV dual side curing temperature and UV dual side curing time were held at 120 °C and 4 s, respectively. The minimum distortion of PSA was with the dot size was between 200 μm to 230 μm and the bottom UV curing time of 0.7 s

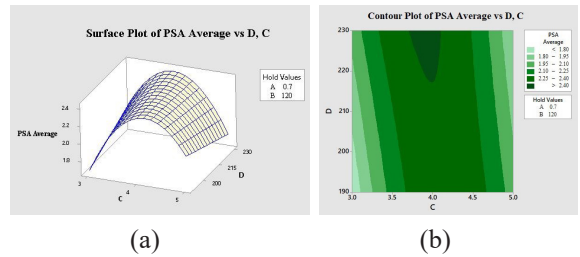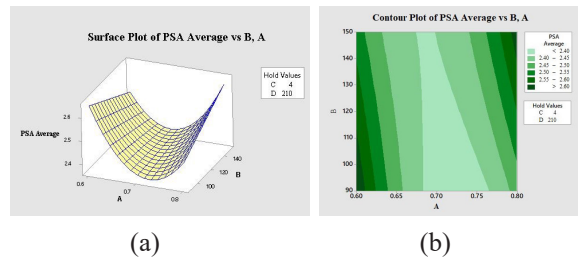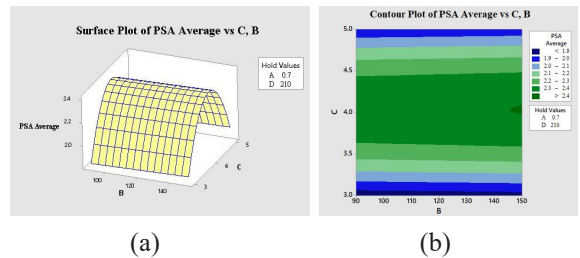The interaction effects between the dot size

(a)   (b)

Figure 16: Relationship between the UV dual side curing temperature and UV dual side curing time on the PSA (a) response surface plot and (b) contour plot.

diameter and the UV dual side curing time on the PSA is presented in Figure 14. It is clear that the proper condition with the minimum PSA distortion was with the dot size of 230 μm and the UV dual side curing time at 5 s.

It is demonstrated in Figure 15 that the minimum distortion of the PSA was at the UV dual side temperature in the range from 100 °C to 140 °C and time of UV bottom curing of 0.7 s.

According to Figure 16 where the UV dual side temperature was set at 100 °C to 140 °C and UV dual side curing time was kept at 3 s, the PSA distortion
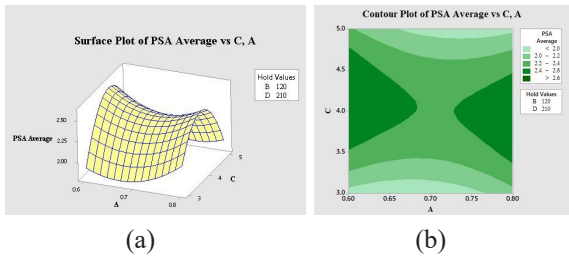
(a)   (b)

Figure 17: Relationship between the UV bottom curing time and UV dual side curing time on the PSA (a) response surface plot and (b) contour plot.

was at the minimum when the dot size and UV bottom curing time were set at 210 μm and 0.7 s, respectively

The response surface plot in Figure 17 shows the combined effect of UV bottom curing time and UV dual side curing time on the PSA. The plots indicate that the time for the UV bottom curing is less sensitive to PSA when the UV dual side curing time was controlled at 3 s.

3.5   *Multi-objective optimization*

The response optimization is shown in Figure 18. The graphs show the nonlinear program (NPL) mathematical model. In HDD manufacturing, both criteria are equally the most important. Therefore, the weight of

the desirability function was considered to be equal to 1. In summary, the process condition parameters used for the optimization of the two responses are: dot size = 230 μm, UV dual side curing temperature = 120 °C, UV dual side curing time = 5 s, UV bottom curing time = 0.7 s. However, the PSA was found to be 0.02 degrees above the target but still within the control limit of 1.78 + 0.2 degree. This satisfies the performance objective. The criteria form of mathematical model optimization and predicted value are summarized in Table 5.

Table 5: Optimal process parameters and predicted values

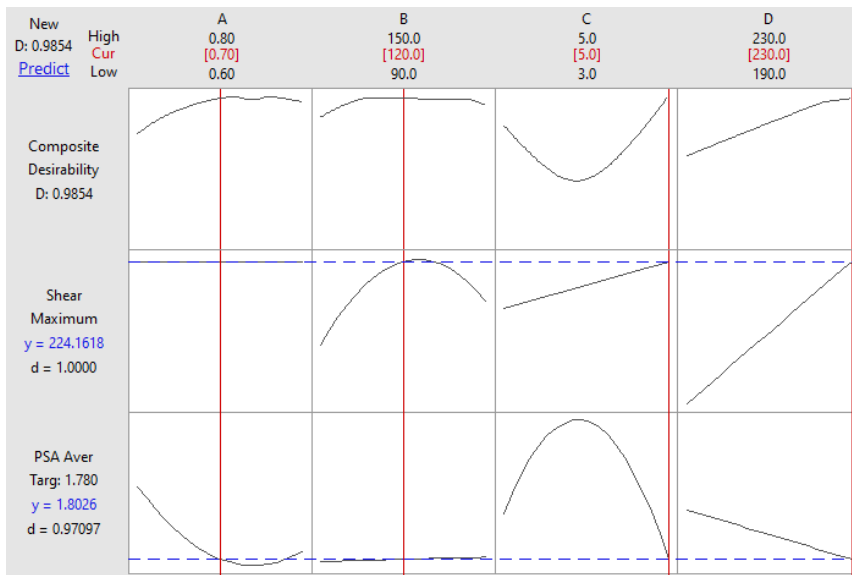| Process Parameter	Unit	Optimal Process Parameter	Predicted Value
UV bottom curing time (A)	s	0.7	-
UV dual side temperature (B)	°C	120	-
UV dual side curing time (C)	s	5	-
Dot size (D)	μm	230	
UV curable epoxy adhesive shear strength force joint	gf	-	224.162
HGA process PSA	degree	-	1.8026

Figure 18: Multi-objective optimization response with the maximum UV curable epoxy adhesive shear strength force joint and PSA with the design fly height target of 1.78 degree.

3.6 *Model validation*

The FCCD approach was applied to evaluate the experiment. To verify the reliability of the mathematical and multi-objective models, tests to compare with predicted values with 200 HGAs were conducted. It is normal that the comparison of the predicted value with the actual value has a small percentage of error. Table 6 presents the error percentage of the actual value and predicted value of the validation experiments. It was found that the percentage value is less than 7%, which was in good agreement in term of HDD criteria requirement. This provides us with confidence in the application of the model and its accuracy. Thus, this validation leads to the importance of the process parameter with respect to the target. Therefore, the new automated UV equipment can ensure the quality of the process through these optimal process parameters.

Table 6: Validation results

Responses	Desirability	Predicted Value	Confirmation Value	Error (%)
UV curable epoxy adhesive shear strength force joint	1.000	224.162	208.92	6.799
HGA process PSA	1.000	1.8026	1.815	0.688

4 Conclusions

The aim of the paper is to maximize the UV curable epoxy adhesive shear strength force joint and PSA to achieve the process target. New technology of UV design for spot quick curing of adhesive has been proposed for the replacement of the conveyorized infrared oven technology. The FCCD concept was applied to determine the relationships of these factors and interactions between these factors. The following conclusions can be drawn from this work:

1) The analysis of variance confirms that the dot size, UV dual side temperature, UV dual side curing time and the quadratic term of the UV dual side temperature are significantly contributed to the UV curable epoxy adhesive shear strength force joint. The UV bottom curing time is not significant.

2) A nonlinear programming (NLP) model, was obtained by the analysis of variance. This second-order model was classified as the NLP model since there are two-way and three-way interaction effects in this regression model. The software was utilized to solve this NLP model. The optimization function yields the optimum process parameters to maximize the shear strength force and PSA to be on process target. The interaction plots and response surface plots were used to confirm the optimization results.

3) The adhesive dot size is recommended to be with the set up at the highest level, the dual side UV temperature at 120 °C, the time duration of UV bottom in the middle levels, and the UV dual side at the higher level to achieve the maximum adhesive shear strength force and attain the PSA target value.

4) The predicted shear strength force joint and PSA value obtained from the optimization algorithm is in good agreement with the validation experiment. The percentage error is only 7%. Therefore, the quadratic model can be used in predicting the PSA with a high confidence level.

5) With the new process parameters, a major improvement on the slider-suspension attachment in the HGA manufacturing process can be achieved. The average UV curable epoxy adhesive shear strength force joint was 208.92 gf and PSA was 1.815 degree.

6) This work has been successfully improved the side effects of the newly designed product platform. The reliability requirements of the new product from the higher UV curable epoxy adhesive shear strength force joint have been satisfied and PSA was close to the target. Therefore, this new product platform can be launched with a high confidence level.

7) This research was limited to the optimization of standard process factors. The adhesive changing was not allowable at the factory level. The changes of adhesive type or adhesive property are another interesting and possible research in the future to improve the adhesive shear strength force. Careful research is important because the outgassing and thermal expansion properties of adhesive after a full cure may change in the extreme temperature and humidity environment. This will lead to a difference in fly height.

References

[1] J. Lin, Z. Lu, H. Yang, and P. Wang, "A design of experiments assessment of moisture content in uncured adhesive on static strength of adhesive-bonded galvanized SAE1006 steel," *International Journal of Adhesion and Adhesives*, vol. 31, pp. 478–485, 2011.

[2] J. LeBono, L. Barton, and M. Birkett, "Low temperature tensile lap-shear testing of adhesively bonded polyethylene pipe," *International Journal of Adhesion and Adhesives*, vol. 74, pp. 57–63, 2017.

[3] S.-W. Lee, J.-W. Park, C.-H. Park, D.-H. Lim, H.-J. Kim, J.-Y. Song, and J.-H. Lee, "UV-curing and thermal stability of dual curable urethane epoxy adhesives for temporary bonding in 3D multi-chip package process," *International Journal of Adhesion and Adhesives*, vol. 44, pp. 138–143, 2013.

[4] R. Aradhana, S. Mohanty, and S. K. Nayak, "A review on epoxy-based electrically conductive adhesives," *International Journal of Adhesion and Adhesives*, vol. 99, 2020, Art. no. 102596.

[5] Ž. Unuk, A. Ivanič, V. Ž. Leskovar, M. Premrov, and S. Lubej, "Evaluation of a structural epoxy adhesive for timber-glass bonds under shear loading and different environmental conditions," *International Journal of Adhesion and Adhesives*, vol. 95, 2019, Art. no. 102425.

[6] J. T. Gruener, A. Vashisth, M. J. Pospisil, A. C. Camacho, J.-H. Oh, D. Sophiea, S. E. Mastroianni, T. J. Auvil, and M. J. Green, "Local heating and curing of carbon nanocomposite adhesives using radio frequencies," *Journal of Manufacturing Processes*, vol. 58, pp. 436–442, 2020.

[7] D. Quan, B. Deegan, L. Byrne, G. Scarselli, A. Ivanković, and N. Murphy, "Rapid surface activation of carbon fibre reinforced PEEK and PPS composites by high-power UV-irradiation for the adhesive joining of dissimilar materials," *Composites Part A: Applied Science and Manufacturing*, vol. 137, 2020, Art. no. 105976.

[8] K. Schmidt and A. Zimmermann, "Evaluation of process and anisotropy of thermosetting adhesives with ultraviolet-assisted 3D dispensing," *Additive Manufacturing*, vol. 34, 2020, Art. no. 101262.

[9] A. N. Rider, C. H. Wang, and J. Cao, "Internal resistance heating for homogeneous curing of adhesively bonded repairs," *International Journal of Adhesion and Adhesives*, vol. 31, pp. 168–176, 2011.

[10] T. Vallée and M. Adam, "Inductively cured glued-in rods in timber using curie particles," *International Journal of Adhesion and Adhesives*, vol. 70, pp. 37–45, 2016.

[11] A. H. Lutey and F. Moroni, "Pulsed laser texturing for improved adhesive-bonded polyethylene (PE) joints," *International Journal of Adhesion and Adhesives*, vol. 102, 2020, Art. no. 102676.

[12] L. Sutherland, C. Amado, and C. G. Soares, "Statistical analyses of the effects of bonding parameters and fabrication robustness on the strength of adhesive T-joints," *Composites Part B: Engineering*, vol. 175, 2019, Art. no. 107063.

[13] P. R. Oliveira, M. May, T. H. Panzera, F. Scarpa, and S. Hiermaier, "Reinforced biobased adhesive for eco-friendly sandwich panels," *International Journal of Adhesion and Adhesives*, vol. 98, 2020, Art. no. 102550.

[14] F. Moroni, L. Romoli, and M. Khan, "Design of laser-textured surfaces to enhance the strength of adhesively bonded joints," *International Journal of Adhesion and Adhesives*, vol. 85, pp. 208–218, 2018.

[15] J. Lasprilla-Botero, M. Álvarez-Láinez, D. A. Acosta, and J. M. Martín-Martínez, "Water-based adhesive formulations for rubber to metal bonding developed by statistical design of experiments," *International Journal of Adhesion and Adhesives*, vol. 73, pp. 58–65, 2017.

[16] J. Deeying, K. Asawarungsaengkul, and P. Chutima, "Multi-objective optimization on laser solder jet bonding process in head gimbal assembly using the response surface methodology," *Optics & Laser Technology*, vol. 98, pp. 158–168, 2018.

[17] B. F. Ryan, B. L. Joiner, and J. D. Cryer, MINITAB *Handbook: Update for Release*. Massachusetts: Cengage Learning, 2012.

[18] D. C. Montgomery, *Design and Analysis of Experiments*. New Jersey: John Wiley & Sons, 2012.